THE EFFECT OF SHEAR ON COLLOIDAL AGGREGATION AND GELATION STUDIED USING SMALL-ANGLE LIGHT SCATTERING

by

TAHEREH MOKHTARI

B.S., Sharif University of Technology, 1998

A REPORT

submitted in partial fulfillment of the requirements for the degree

MASTER OF SCIENCE

Department of Physics
College of Arts and Sciences

KANSAS STATE UNIVERSITY
Manhattan, Kansas

2007

Approved by:

Major Professor
Chris Sorensen

Abstract

We investigated the effect of shear on the structure and aggregation kinetics of unstable colloids using small angle light scattering. We used an aqueous suspension of 20 nm polystyrene latex microspheres and $MgCl_2$ to induce aggregation. The sample was only sheared once for approximately 33 seconds at different times, typically 1 min., 5 min., or 15 min., after the onset of aggregation. The average shear rate was in the range of 0.13 - 3.56 s^{-1}, which was in a laminar regime. The unsheared sample gelled after ca. 45 min. When the sample was sheared soon after the onset of aggregation, the aggregation followed DLCA kinetics to yield D_f = 1.80 ± 0.04 aggregates unaffected by the shear. The gel time also remained the same as the unsheared gel. Shearing at later stages of aggregation shortened the gel time and enhanced the scattered light intensity significantly indicating rapid growth. Then, depending on the shear rate, there were three different behaviors. At high shear rates, the aggregate structure was inhomogeneous after the shear was stopped with a crossover in slope in the scattered light intensity vs. q, to imply hybrid superaggregates with two different fractal dimensions. At intermediate shear rates far from the gel point, there was a similar crossover after the shear was stopped; however, the fractal dimension regained 1.80 ± 0.04 at the gel point. At low shear rates, the aggregation rate was increased, but the aggregate structure was uniform, and the fractal dimension remained 1.75 ± 0.05.

Table of Contents

List of Figures

List of Tables

CHAPTER 1 - INTRODUCTION

The aggregation of small particles to form larger structures is fundamental for aerosols and colloids, and is considerably important in many areas of science and technology [1]. The coagulation of particles depends on their motion. Brownian motion, which is driven by thermal energy, is always present to cause aggregation. Other important mechanisms to create relative motion include gravitational settling, shear, and turbulence.

Many experimental and theoretical studies have been carried out to investigate the effect of shear flow on the kinetics of aggregation, the resulting size distributions, and structures of particle aggregates. Here, we shortly review some of the previous studies done related to the presented paper.

In previous shear experiments the particles first aggregated due to shear, however, these aggregates eventually have either fragmented due to shear [2-6], restructured [6-10] or have experienced both fragmentation and restructuring [10-12]. For example, Serra et al. [2] studied the effect of continuous shear flow on the mean aggregate size. They used polystyrene particles with diameters of 2 μm and 5 μm. The range of the shear rates was 25-195 s^{-1}. They found that the larger the shear, the faster the aggregation occurred; the system reached steady state more rapidly, and the final aggregate size was smaller. They concluded that the shear fragmentation eventually balanced the aggregation, and a steady state was then reached. Selomulya et al. [6] found that at shear rates less than 100 s^{-1} restructuring of aggregates was favored over fragmentation for aggregates composed of 60 and 380 nm particles, whereas fragmentation and reaggregation were the main mechanism in governing the final floc size and structure for aggregates made up from 810 nm particles. Jung et al. [10] formed iron hydroxide flocs while continuously shearing. They found that at low shear rates the flocs restructured but did not breakup. At high shear rate, however, the flocs fragmented and restructured, and became small and compact with a fractal dimension of approximately $D_f = 2.71$.

The fractal dimension of the shear induced aggregates has been shown either to be independent of the shear rate for nonzero shear [3-5, 11, 12, 15] or dependent on the shear rates, i.e., high shear rates caused higher fractal dimensions [7-10, 16]. The fractal

dimension of the aggregates in these shear studies ranged from 2.05 - 2.8 [4, 5, 7-12, 15, 16].

In most previous studies [2-6, 10-12, 15, 16], the effect of shear was studied in the continuous presence of shear and in the cluster dilute regime. We define the cluster dilute regime as when the distance between neighboring particulates is much larger than their characteristic size. Furthermore, the shear aggregation in these studies was dominant over Brownian aggregation as quantified by the Péclet number Pe.

In the work presented in this paper we studied a colloid with small primary particles, 20 nm, but at high enough volume fractions so that after approximately 45 min. the system gelled in the absence of shear. We applied the shear for only a short period of time, i.e., 33 s, during the aggregation. We studied the effect of the shear both in the cluster dilute and cluster dense regimes. The cluster dense regime is when the aggregate sizes are comparable to the mean nearest neighbor distance R_{nn}. We studied the effect of the shear for both $Pe < 1$, corresponding to when Brownian aggregation is dominant, and $Pe > 1$, corresponding to when the shear aggregation is dominant. To observe the aggregation, *in situ* light scattering measurements were carried out both before and after initiating the shear. This allowed us to study both the kinetics of aggregation and the structure of the aggregated particles. Unlike previous work we find no evidence for restructuring or fragmentation during shear for our colloid. Instead shear always caused enhanced aggregation when the Péclet number was greater than one. Shear applied far away from the gel point yielded aggregation with a fractal dimension of 1.8. Near the gel point in the cluster dense regime, however, shear induced growth of the $D_f = 1.8$ aggregates into hybrid structures with a fractal dimension of ca. 2.6 over large length scales and 1.8 over smaller scales. We interpret this to indicate the shear induced formation of hybrid superaggregates, large aggregates of a given fractal dimension formed from smaller aggregates of a different fractal dimension. This observation of hybrid superaggregates is consistent with previous simulations and experiments with flame soot aerosols [17, 18, 19].

CHAPTER 2 - EXPERIMENTAL METHODS

The experiments were performed with surfactant-free nearly monodisperse polystyrene latex spheres with a diameter of d = 20 nm (12% coefficient of variance), purchased from IDC [20, 21]. Magnesium chloride salt ($MgCl_2$) was used to screen the Coulombic potential of the initially charge stabilized polystyrene particles and thus induced the aggregation. In all experiments the final molarity of the $MgCl_2$ solution was 10.12 mM, and the final volume fraction of the polystyrene particles was 4.36×10^{-4} [20]. We chose a salt concentration large enough to ensure that the aggregation kinetics was controlled via diffusion limited cluster-cluster aggregation (DLCA) kinetics. The polystyrene and $MgCl_2$ solutions were prepared in a mixture of H_2O and D_2O in order to match the density of polystyrene (1.05 g/cm^3), hence to prevent the collapse of the tenuous network due to gravity [20, 21]. We used equal volumes of the polystyrene particle suspension and $MgCl_2$ solution to prepare the samples for light scattering. The two solutions were simultaneously squirted into the cell (described below) through holes in the O-ring with 50 µl syringes. There was a bubble present in the cell, which was approximately 0.14 of the total volume of the cell. The mixing time, a few seconds, was negligible compared to the gel time, which ensured that mixing would not disturb the aggregation kinetics.

As shown in Fig. 1, the cell was made of one silicone O-ring (d = 9 mm) sandwiched between two 23 mm-diameter quartz windows. The sample was sealed inside a metal sample holder, which had a hole centered on the quartz windows. The spacing between the windows, hence the optical path length of the cell, was 1.8 mm. The sample holder was then mounted onto a sample rotator. The axis of rotation of the sample holder, hence the angular velocity vector ω, was parallel to the direction of the incident laser beam, perpendicular to the windows. We varied the rotation rate of the sample holder by altering the voltage of a DC gear motor.
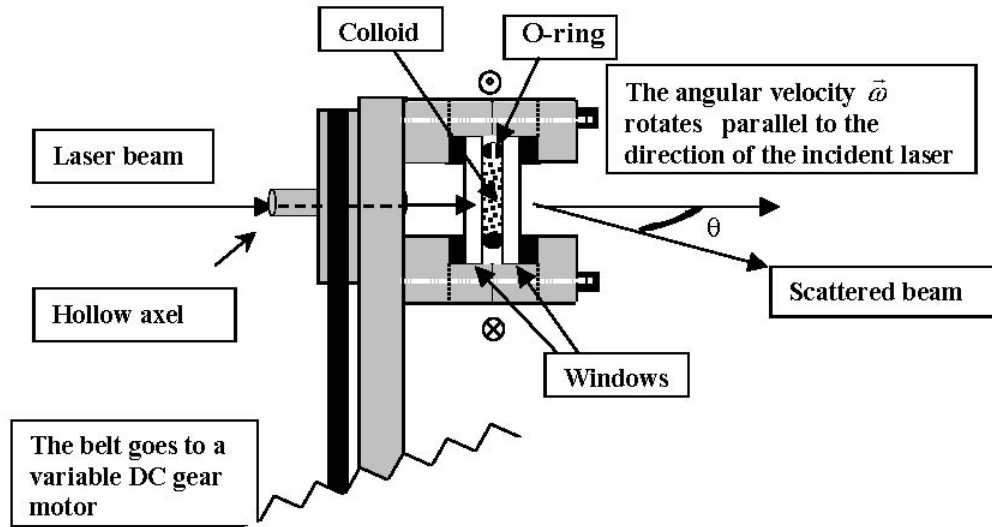
Figure 1: Schematic diagram of the sample rotator.

In order to compute the shear rate, the rotational aggregation chamber was simulated using the computation fluid dynamics software FLUENT 6.2.12. The volume of fluid (VOF) model was chosen to describe the air-water multi-phase system. The detailed simulation settings are reported in Table 1 When the flow field was computed, the average shear rate was obtained by integrating over the liquid phase. It is also noted that, at the interface, the computed shear rate is evidently high because of the large difference between velocities in the liquid and gas phases. Therefore, the shear rate was averaged excluding the interface. In the experiments presented here, the rotational speed was varied between 0.085 rad/s $\leq \omega \leq$ 2.83 rad/s, corresponding to the simulated shear rate of 0.13 s$^{-1} \leq \overline{G} \leq$ 3.56 s^{-1}.

Solver	2nd-order implicit, segregated, unsteady, variable time steps, cell-based gradient
Grid Size	Cells 9,414 / Faces 29,558 / Nodes 10,770
Multi-phase model	Volume of Fluid (VOF) / Geo-Reconstruct scheme
Viscous model	Laminar

Table 1: CFD Simulation Condition Settings in Fluent 6.2.12.

We began shearing the samples at different times after the onset of aggregation. We defined this time as the *shear initiation time,* which was typically 1, 5 and 15 min. after the onset of aggregation. We also sheared samples at higher shear rates (2.61 and 3.56 s^{-1}) for the shear initiation time of 3 min. We defined the time that the samples were sheared as the *shear duration time*, which was 33 ± 3 s. The light scattering measurements were taken both before the shear was applied, and after the shear was stopped. The samples were sheared only once. We should also note that we empirically observed that after the shear was stopped, the structure of the aggregates did not depend on the position of the laser beam. There was enough mixing during the shear so we were not concerned about the position of laser beam on the cell. However, we still had the laser beam mostly on the lower half of the cell during our experiments.

The relative importance of shear-induced aggregation compared to Brownian aggregation is quantified by the Péclet number

$$Pe = \frac{R_p^2 \overline{G}}{D}.$$ (1)

In Eq. (1), R_p is the perimeter radius of the aggregates when two clusters collide due to shear, and D is the translational diffusion coefficient given by

$$D = \frac{k_B T}{6\pi\eta R_m}.$$ (2)

In Eq. (2), η is the solvent viscosity ($\eta = 8.90 \times 10^{-4}\, kg/ms$), k_B is the Boltzmann constant ($k_B = 1.38 \times 10^{-23}$ J/K), T is the ambient temperature (T = 298 K), and R_m is the mobility radius of the aggregates.

For simplicity, we arbitrarily used the aggregate radius of gyration, R_g for both R_p and R_m to determine the Péclet number. By substituting Eq. (2) into Eq. (1) and using R_g in these equations ($R_g \propto R_m \propto R_p$), we obtain

$$Pe = \frac{6\pi\eta R_g^3 \overline{G}}{k_B T}. \qquad (3)$$

The R_g is the measured size of the aggregates immediately before applying the shear.

The design of our SALS apparatus was based on that of Ferri [22]. We used a vertically polarized argon-ion laser (Spectra Physics, model 165) operating at a wavelength of $\lambda_\circ = 488$ nm. The laser beam is scattered by the sample. The scattered light is collected by a lens (Achromat F=75 mm, ϕ=50.8 mm). A mirror, made of a 0.6 mm drill tip cut and polished at 45°, is placed in the focal plane of this lens, which deviates the transmitted beam to 90°. The scattered light focused in the focal plane of first lens is conjugated by a second lens (Achromat F=100 mm, ϕ=50.8 mm) onto a photodiode array. The scattered light intensity was measured vs. the scattered angle. The range of angles for the SALS experiments was $0.18^\circ \le \theta \le 13.4^\circ$ corresponding to wave vectors of $400\ cm^{-1} \le q \le 3 \times 10^4\ cm^{-1}$, where

$$q = (4\pi/\lambda_m)\sin(\theta_m/2). \qquad (4)$$

Note that in Eq. (4), both λ_m and θ_m should be considered inside the cell in the aqueous medium.

The background intensity was measured immediately after placing the sample on the sample holder, i.e., before any aggregation. The background intensity which was very small fraction of the scattered intensity, then subtracted from subsequent light scattering measurements.

In order to determine the radius of gyration of the clusters, we used the Guinier analysis [23]. The Guinier equation, may be expressed as

6

$$I(0)/I(q) \cong 1 + \frac{1}{3}R_g^2 q^2 . \tag{5}$$

The Guinier analysis proceeds by plotting the inverse, normalized scattered intensity vs. q^2. The plot should be linear, with a slope equal to $R_g^2/3$ when $qR_g < 1$. The range of scattering angles in our experiment limited the aggregate size range that we could detect to 0.3 μm $< R_g <$ 25 μm.

When $qR_g > 1$, the scattering enters a power law regime and if the aggregates are fractals, $I(q) \approx q^{-D_f}$, where D_f is the fractal dimension of the aggregates. Thus log-log plots of $I(q)$ vs. q have a slope of $-D_f$.

CHAPTER 3 - RESULTS AND DISCUSSION

In order to study how shear affects the aggregation kinetics and the structure of the aggregates, we took baseline light scattering measurements with no shear, i.e., with Brownian aggregation. Figure 2 shows a sequence of the scattered intensities plotted vs. q at various times after the onset of aggregation. The static light scattering stopped evolving after about 45 ± 5 min., indicating that a space-filling network of fractal clusters had formed. We defined that the gel time occurred when the light scattering intensities stopped evolving, i.e., there was no further aggregation. The fractal dimension was $D_f = 1.78 \pm 0.03$, consistent with the DLCA aggregation process.
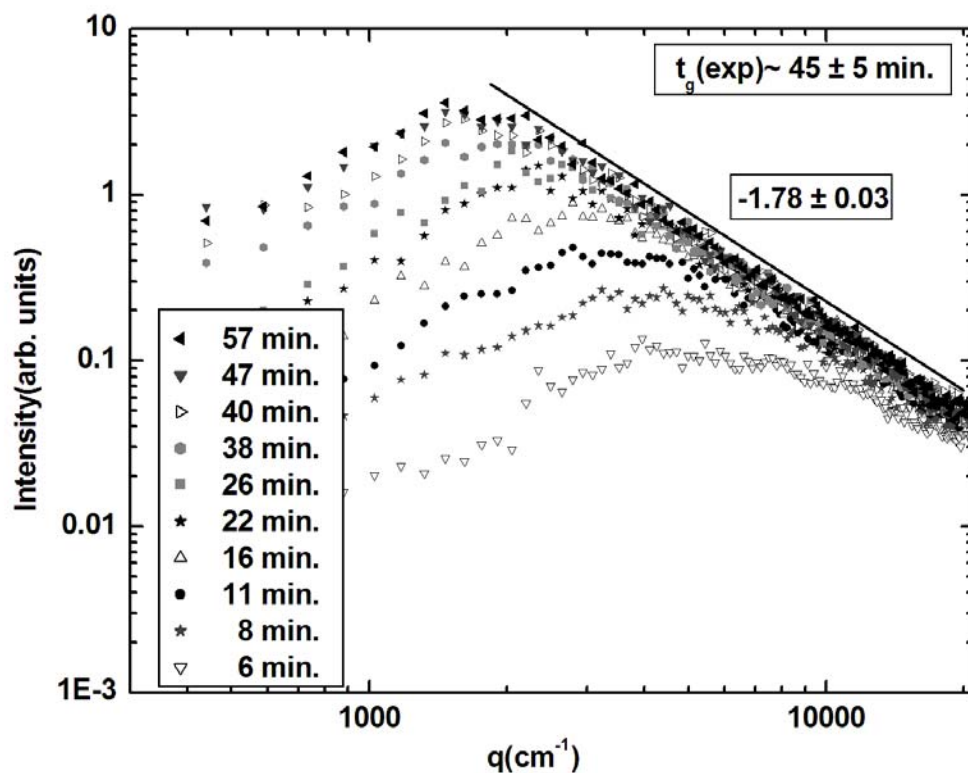

Figure 2: Static light scattering intensities (arbitrary units) plotted vs. q (cm^{-1}) at various times after the onset of aggregation. Curves are labeled by the time elapsed after initiating the aggregation. Gelation occurred at about 45 ± 5 min. The fractal dimension is $D_f = 1.78 \pm 0.03$.

The peak in $I(q)$ vs. q which has been observed previously [21, 24-26] can be described as follows. The total structure factor is a combination of the single-cluster structure factor and the cluster-cluster structure factor. The characteristic length scale of the single-cluster structure factor is R_g, while the length scale of the cluster-cluster structure factor is the mean nearest neighbor distance R_{nn}. This product causes an apparent peak in the structure factor when the aggregating system is dense enough that the two length scales are comparable in magnitude [27, 28, 29].

In Fig. 3, the scattered intensities are plotted vs. q at different times before and after initiating the shear, which was $\overline{G} = 0.99$ s^{-1}. The shear initiation time was 1 min. As shown in this figure, there are no changes in the light scattering intensity due to the shear. This indicates that the shear did not affect the kinetics of aggregation. The sample aggregated based on Brownian aggregation, just as it would if the sample had not been sheared at all. The sample gelled within 50 ± 10 min. with a fractal dimension of $D_f =$ 1.80 ± 0.04, essentially the same values within error as the no shear situation alone.

In Table 2 we summarize the results, including the gel time, t_g, and the fractal dimension for the shear initiation time of 1 min. at different shear rates. As shown in Table 2, at all shear rates, the gel time remained more or less the same as when there was no shear (Fig. 2). The negative slope also remained 1.80, which is the fractal dimension of the aggregates in the DLCA aggregation regime. The Péclet number was less than one at all shear rates. We also observed each sample visually after it reached its gel point. The gel structure was uniform and similar to the gel formed with no shear.

Figure 3: Static light scattered intensities (arbitrary units) plotted vs. q (cm^{-1}) at different times before and after initiating the shear. The shear rate was $\overline{G}$ = 0.99 s^{-1}. The shear initiation time was 1 min. Gelation occurred at about 50 ± 10 min. The fractal dimension is D_f = 1.80 ± 0.04.

$\overline{G}$ (s^{-1})	D_f	t_g (min.)
0.13	1.80	40 ± 5
0.24	1.80	40 ± 5
0.48	1.80	35 ± 5
0.99	1.80	50 ± 10
1.60	1.78	45 ± 10
2.61	1.80	40 ± 10
3.56	1.80	45 ± 10

Table 2: Gel time and fractal dimension for the shear initiation time of 1 min at shear rates ranged from 0.13- 3.56 s^{-1}. The error in the fractal dimension is approximately 0.04.

Figure 4 shows the scattered intensities vs. q at different times before and after initiating the shear, when the shear initiation time was 3 min., and the shear rate was $\overline{G} = 2.61$ s^{-1}. As indicated by the arrow, there was a large jump in the light scattering intensity after the shear was stopped indicating that the shear enhanced the aggregation. Moreover, there was a crossover between two different negative slopes of 0.95 ± 0.04 and 2.10 ± 0.04, implying that the aggregate structure was inhomogeneous. These two slopes indicate two different aggregate structures at different length scales. We believe that the negative slope of 0.95 at higher q does not have any quantitative significance, because we were limited in our ability to detect the scattering intensity at larger scattering angles to detect the power law regime, which could have a negative slope of 1.8. After the shear was stopped, Brownian aggregation eventually overcame the shear-induced double structure and "repaired" the clusters over time, until the sample gelled with a more tenuous structure, which had a fractal dimension of 1.80 ± 0.04. The Guinier analysis showed some slight decrease in the aggregate size after the shear was stopped all throughout the completion of the gelation. We call this post shear aggregate restructuring. A rough calculation shows that if these fairly compact $D_f = 2.1$ aggregates changed to a more tenuous $D_f = 1.8$ aggregates, the aggregate radius of gyration should have become approximately 3 times larger. However, our results do not show any increase in the aggregates' size. Thus, the disappearance of the double structure is perplexing and remains yet a question.

The gel time in Fig. 4 is 20 ± 4 min., which is shorter than the gel time of the unsheared sample, another evidence for the shear enhanced aggregation.
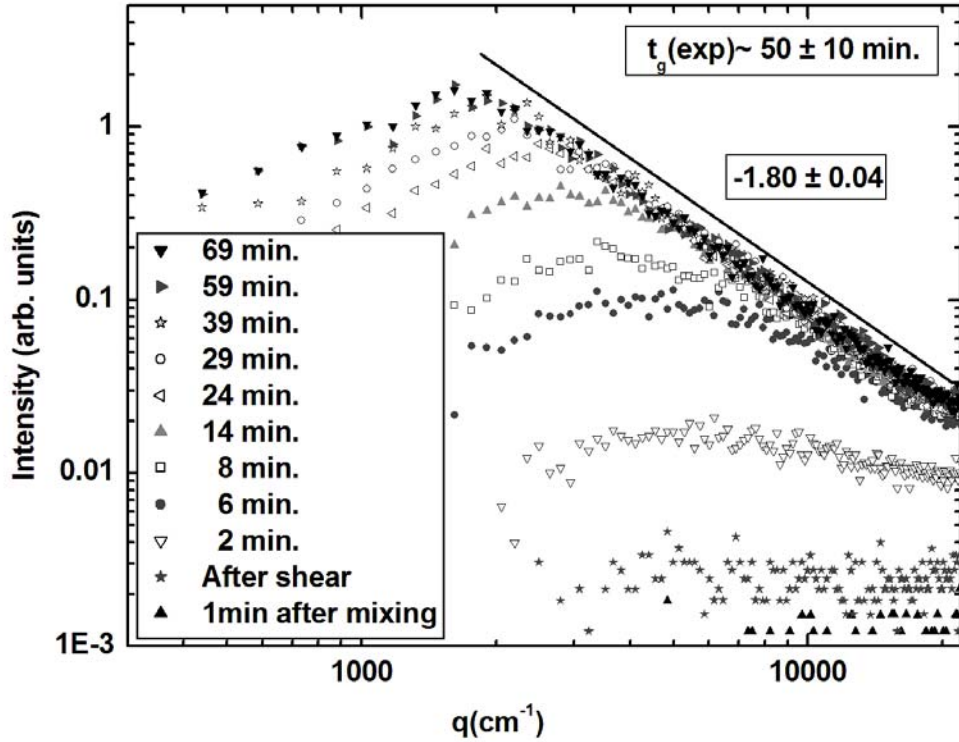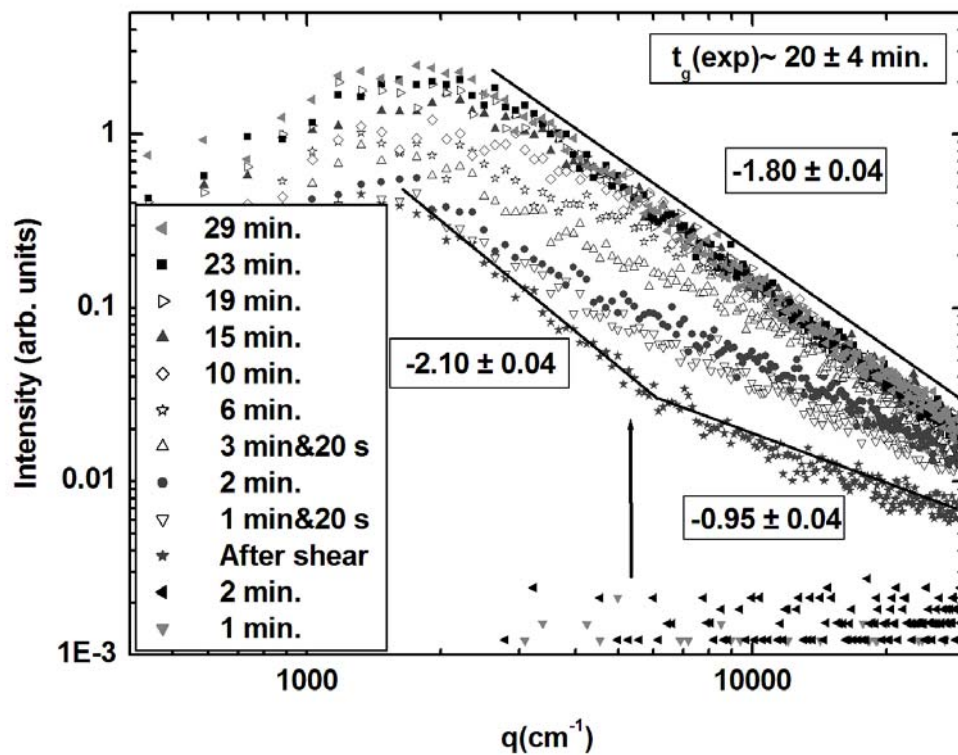
Figure 4: Static light scattered intensities (arbitrary units) plotted vs. q (cm^{-1}) at different times before and after initiating the shear. The shear rate was $\overline{G}$ = 2.61 s^{-1}. The shear initiation time was 3 min. Gelation occurred at about 20 ± 4 min. There is a crossover between two different slopes of D_f = 0.95 ± 0.04 and D_f = 2.10 ± 0.04 evolving to 1.80 ± 0.04.

For the shear initiation time of 5 min. we observed three different behaviors, which depended on the applied shear rates. The Péclet number was greater than one at all shear rates. These results are shown in Table 3 and are as follows:

$\overline{G}$ (s^{-1})	D_f	t_g (min.)
0.13	1.80	40 ± 5
0.24	1.80	40 ± 5
0.48	1.80	35 ± 5
0.99	1.80	50 ± 10
1.60	1.78	45 ± 10
2.61	1.80	40 ± 10
3.56	1.80	45 ± 10

Table 3: Gel time and fractal dimension for the shear initiation time of 5 min. at shear rates ranged from 0.13-3.56 s^{-1}. The error in the fractal dimension is approximately 0.03.

At low shear rates ($\overline{G} = 0.13$ s^{-1}-0.99 s^{-1}), of which we show an example in Fig. 5; shear enhanced the aggregation as indicated by the arrow. Once again in this figure, we plotted the scattered intensities vs. q at different times before and after initiating the shear. The shear rate was $\overline{G} = 0.13$ s^{-1}. After the shear was stopped, Brownian motion continued the aggregation until the sample gelled with a fractal dimension of 1.71. The gel time was 30 ± 5 min., which was shorter than when there was no shear.

As the shear rate increased to 1.66 and 2.61 s^{-1}, the shear enhanced the aggregation and caused a crossover in the slope in the scattered intensity vs. q similar to Fig. 4. Likewise, Brownian aggregation "repaired" this double structure into a uniform gel. The fractal dimension regained 1.83, which is also similar to Fig. 4. The gel time was approximately 14 ± 4 min., which again was shorter than the gel time when there was no shear and the smaller shear rates.

13

When we increased the shear rate to 3.56 s^{-1}, not only did the shear enhance the aggregation, but it also caused the sample to reach its gel point. The gel time was significantly shorter, t_g = 6 ± 1 min., compared to the no-shear situation and the smaller shear rates. The shear also once again caused two different slopes in the scattered intensity vs. q, and this shear-induced double structure remained after gelling was completed.
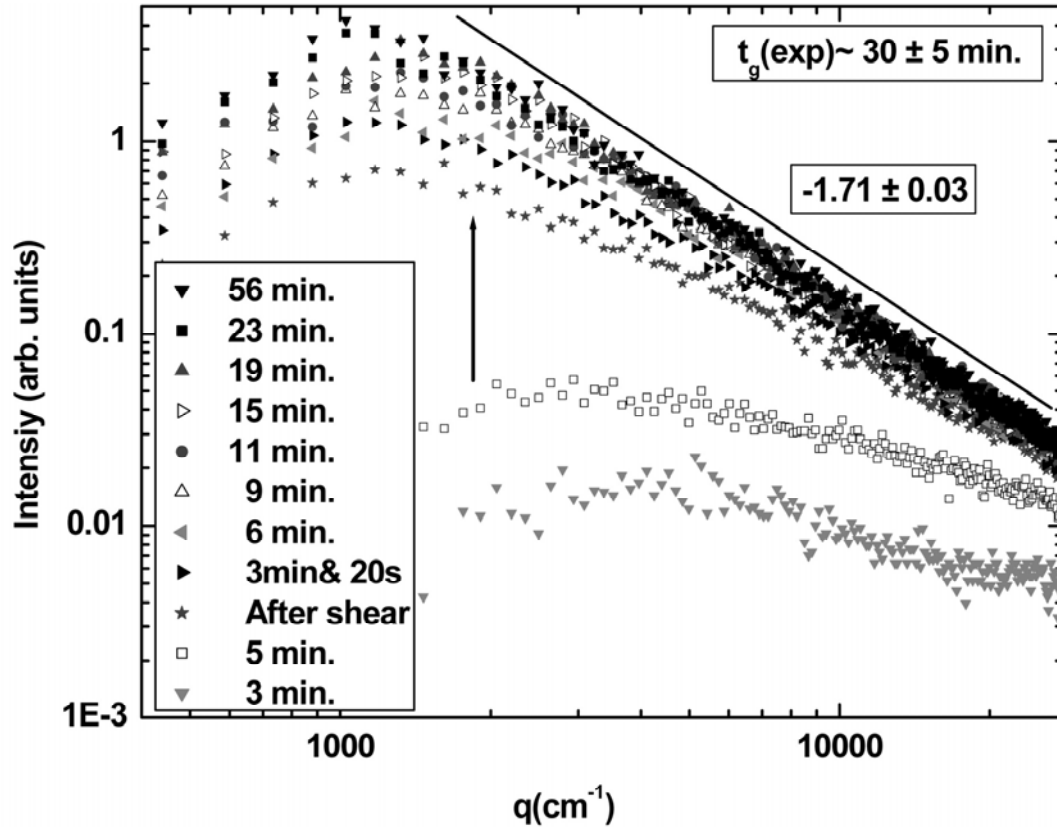

Figure 5: Static light scattered intensities (arbitrary units) plotted vs. q (cm^{-1}) at different times before and after initiating the shear. The shear rate was $\overline{G}$ = 0.13 s^{-1}. The shear initiation time was 5 min. Gelation occurred at about 30 ± 5 min. The fractal dimension is D_f = 1.71 ± 0.03.

We also studied the situation when the shear initiation time was 15 min. These results are shown in Table 4. At shear initiation time of 15 min., the shear enhanced the aggregation at all shear rates similar to the results described for the shear initiation time of 5 min. However, we found that the shear-induced double structure at the gel point occurred at a lower shear rate, $\overline{G} = 0.48$ s^{-1}, compared to $\overline{G} = 3.56$ s^{-1} for the shear initiation time of 5 min. The sample gelled due to the shear aggregation within 16 ± 1 min. (one minute past the shear initiation time) at all shear rates but the lowest shear rate for which the gel time was 18 ± 2 min. The Péclet number was well above one at all shear rates. Comparing the results of Tables 3 and 4 suggests that as the shear initiation time increased, the shear rate needed to cause the double structure shifted to a smaller value. Table 5 briefly summarizes and highlights the results of Tables 2, 3, and 4.

$\overline{G}$ (s^{-1})	D_f	t_g (min.)
0.13	1.75	18 ± 2
0.24	1.75	16 ± 1
0.48	1.75 & 2.60	16 ± 1
0.99	1.75 & 2.55	16 ± 1
1.60	1.65 & 2.61	16 ± 1
2.61	1.60 & 2.52	16 ± 1
3.56	1.73 & 2.45	16 ± 1

Table 4: Gel time and fractal dimension for the shear initiation time of 15 min at shear rates ranged from 0.13- 3.56 s^{-1}. The error in the fractal dimension is approximately 0.04.

Shear initiation time (min.)	Shear rate (s^{-1})	Shear effect
No shear	N/A	Uniform gel structure: $D_f \approx 1.8$ Gel time 45 ± 5 min.
1	$0.13 \leq \overline{G} \leq 3.56$	Uniform gel structure: $D_f \approx 1.8$ Gel time 42 ± 8 min.
5	$0.13 \leq \overline{G} \leq 0.99$	Enhanced shear aggregation Uniform gel structure: $D_f \approx 1.8$ Gel time 25 ± 5 min.
	$1.60 \leq \overline{G} \leq 2.61$	Enhanced shear aggregation Hybrid aggregate structure after shear was stopped Uniform gel structure Gel time 14 ± 4 min.
	$\overline{G} \approx 3.56$	Enhanced shear aggregation Hybrid gel structure Gel time 6 ± 1 min.
15	$0.13 \leq \overline{G} \leq 0.24$	Enhanced shear aggregation Uniform gel structure: $D_f \approx 1.8$ Gel time 16 ± 1 min.
	$0.48 \leq \overline{G} \leq 3.56$	Enhanced shear aggregation, Hybrid gel structure, Gel time 16 ± 1 min.

Table 5: Summary of the shear effects for the shear initiation times of 1, 5, and 15 min. at shear rates ranged from 0.13- 3.56 s^{-1}.

In order to get more insight into the aggregation growth at different shear rates and shear initiation times, we used Guinier analysis [23] to determine the radius of gyration vs. time in each run. The results for the shear rates of 0.13, 0.99, 2.61 and 3.56 s^{-1} are shown as examples in Figs. 6(a), 6(b), 6(c) and 6(d), respectively. The horizontal dashed line in Fig. 6 shows the lower limit of our SALS in measuring the aggregate size (ca. 300 nm). In all these figures, the data are shown for the no shear situation and the shear initiation times of 1, 5 and 15 min. For higher shear rates of 2.61 and 3.56 s^{-1}, we have also shown the result for the shear initiation time of 3 min.

We should first point out the similarities among all these graphs which is as follows: For the shear initiation time of 1 min. and regardless of the shear rates, the data followed, within error, the same curve as the no shear situation up to the gel point. The final aggregate size for both shear initiation time of 1 min. and the no shear case was ca. 4 μm. As the shear initiation time increased to 3, 5, and 15 min. the data, before applying the shear, followed the same curve as the no shear situation. However, after the shear was stopped, the size of the aggregates enhanced to a larger aggregate size (shown by the arrows), and the data followed different curves depended on the shear initiation time and the shear rates. At higher shear rates (2.61 and 3.56 s^{-1}) and for the shear initiation times of 5 and 15 min, the size of aggregates enhanced to a larger size compared to the lower shear rates (0.13 and 0.99 s^{-1}). Moreover, for the shear initiation times of 5 and 15 min., the radius of gyration at gel point was slightly larger (5-6 μm) compared to the shear initiation times of 1 and 3 min., and the no shear situation (4 μm). This difference in the aggregate size could be due to some experimental error or could have some significant meaning, which needs to be investigated more in our future work. As we mentioned before (Table 3, 4), and now we see it more clearly, the gel time was shorter at higher shear initiation times. Once again, the gel time can be found when the aggregate size stops evolving and the data reach a plateau in Fig. 6.
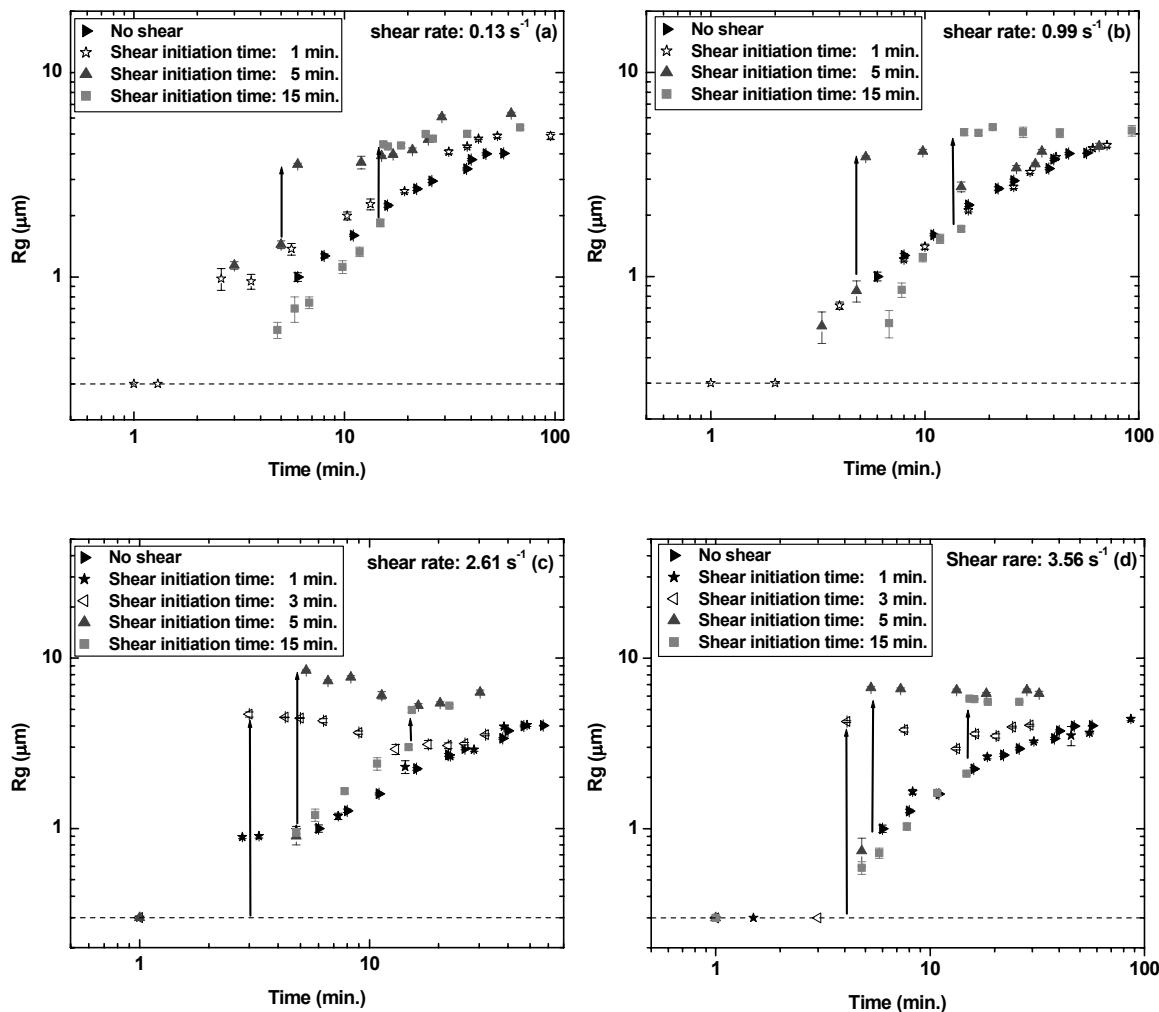
Figure 6: The radius of gyration R_g (µm) plotted vs. time for the no shear situation and the shear rates of (a) 0.13 s^{-1}, (b) 0.99 s^{-1}, (c) 2.61 s^{-1} and (d) 3.56 s^{-1} at different shear initiation times of 1, 3, 5 and 15 min.

We should also note that we had slightly different trend when there was a "double structure" repaired by Brownian aggregation shown previously (Fig. 4): In Fig. 6(b) for the shear initiation time of 5 min. and Fig. 6(c) and 6(d) for the shear initiation time of 3 min., we see that after the shear was stopped, there is a large jump in the aggregate size. However, the aggregates start to slightly decrease in size until they find their stable aggregate size.

Based on our results shown in Table 3 and 4, we conclude that shear can change the uniform aggregate structure to an inhomogeneous structure, which is dependent on both the shear rate and the shear initiation time. In order to emphasize how shear affects the structure and the size of the aggregates, we show as an example in Fig. 7 only the scattered intensities before and after initiating the shear, $\overline{G}$ = 0.48 s^{-1}. The shear initiation time was 15 min. As indicated by the vertical arrow, the shear has enhanced the aggregation, while at the same time the horizontal arrow shows that the radius of gyration has shifted to the smaller q corresponding to the larger aggregate size. This new shear induced structure between the arrows has an effective fractal dimension of 2.6, and over the entire range of q, the two slopes imply a hybrid structure. Thus the questions we now address are what are the conditions and what is the mechanism which causes these hybrid structures?

All previous work implied that there were two possible consequences of shear besides growth: fragmentation [2-6] and restructuring [6-10].

1. Fragmentation: Shear can cause the aggregates to break hence become smaller. Much of the previous work involved both shear aggregation for growth and shear fragmentation, which competed to yield an equilibrium size. Our results, however, showed no indication of fragmentation. Instead the aggregate radius of gyration increased. For example, in Fig. 7 from $R_g \approx 2.8$ μm before applying the shear to $R_g \approx 7$ μm.

2. Restructuring: Another possibility is that the fractal aggregates bend or deform due to shear. Restructuring would tend to occur on larger length scales, hence at low q, where the floc structure is weaker and the hydrodynamic force is larger. In a work relevant to our studies, Lin *et al*. [7] studied the effect of shear on colloidal gold aggregates using static light scattering. They found that shear stress caused two different slopes, hence two different fractal dimensions, in the scattered intensity vs. q. At small q, the slope of the scattering increased markedly with increasing shear, and at large q the scattering still had the same slope as that from unsheared clusters. Lin *et al*. concluded that shear stress caused aggregates formed by Brownian aggregation to restructure towards a higher fractal dimension

19

hence to a smaller aggregate size. In contrast, our results did not show any decrease in the aggregate size due to the shear, instead the size increased. For example, we once again refer to Fig. 7, where we see the shear caused an increase in the fractal dimension but also an increase in the cluster size, not a decrease as expected for restructuring. Lin *et al.* also concluded that the degree of restructuring depended on the magnitude of the shear applied. In contrast, our results again did not show any increase in the fractal dimension as the shear rate increased and the fractal dimension remained more or less the same independent of the applied shear rate.

In summary, we see no evidence for fragmentation or restructuring due to the shear in our data. Moreover, the previous literature has no evidence for shear causing growth to a hybrid structure.

Recently, in work from this laboratory [17] soot aggregates in an acetylene/air laminar diffusion flame were studied using small angle light scattering. An inhomogeneous aggregate structure was observed at higher heights above the burner orifice, i.e., late aggregation times. This structure was similar to Fig. 7 with two different slopes of -1.8 and -2.6 in the light scattering intensity vs. q.

We proposed that this hybrid structure of the flame soot was an indication of superaggregates, a term coined to mean a large aggregate of a given fractal dimension over large length scales composed of smaller aggregates with a different fractal dimension for their smaller length scale. This proposition was based on simulation studies from this laboratory, which showed that DLCA can proceed creating $D_f = 1.8$ fractal aggregates until the system becomes cluster dense [18]. Cluster dense is when the cluster mean nearest neighbor separation becomes comparable to the cluster size. This state will eventually occur in all aggregating systems that create aggregates with a fractal dimension less than the spatial dimension. Once cluster dense, the aggregation mechanism can cross over to a percolation mechanism and $D_f = 2.55$ percolated superaggregates (of smaller $D_f = 1.8$ DLCA aggregates) result [30-33].
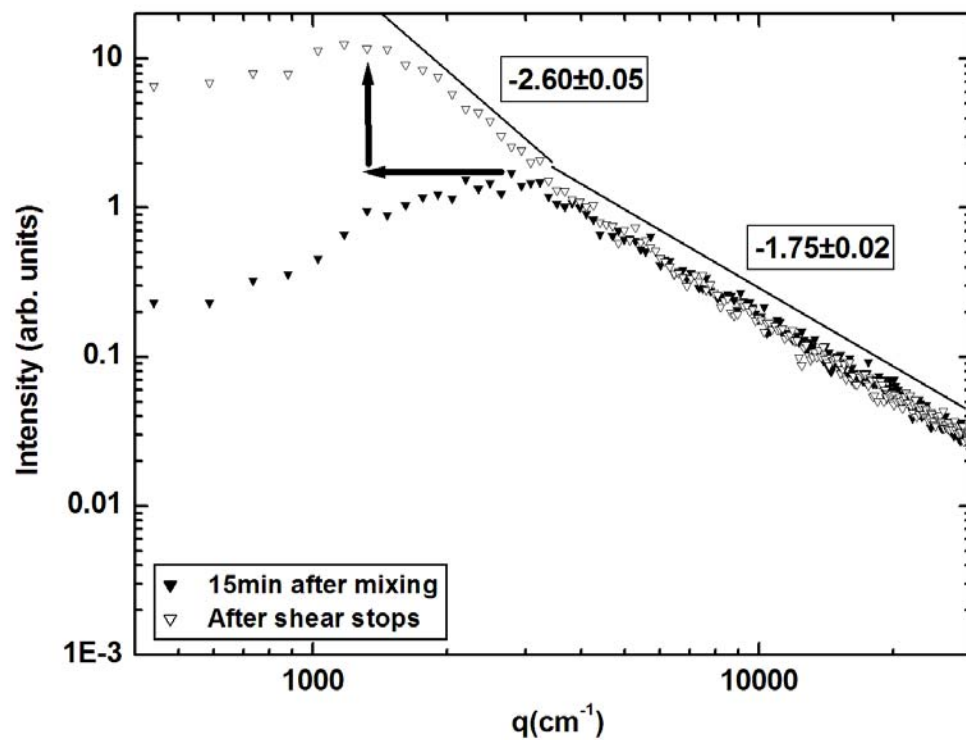
Figure 7: Static light scattered intensities (arbitrary units) plotted vs. q only before and after initiating the shear, $\overline{G}$ = 0.48 s^{-1}. The shear initiation time was 15 min. There is a crossover between two different slopes of D_f = 1.75 ± 0.02 and D_f = 2.60 ± 0.05. The arrows indicate that the aggregate radius of gyration has increased due to the shear.

This mechanism fits our experiments here well. The cross over length scale between the $D_f = 1.8$ and 2.55 morphologies is the size to which the DLCA, $D_f = 1.8$ aggregates have grown when they percolate together into a space filling network, i.e., a gel. This size can be calculated given that at this point the mean monomer number density in the aggregates equals the mean monomer number density across the entire system. We call this cluster size the radius of gyration at the ideal gel point $R_{g,G}$, and it is given by

$$R_{g,G} \approx 0.5\, a\, f_v^{1/(D_f-3)}, \qquad\qquad (6)$$

We use the term "ideal" because we assume spherical clusters all the same size. Given our monomer volume fraction $f_v = 4.36\times10^{-4}$ and size a = 10 nm, we calculate $R_{g,G} = 2.4$ μm for $D_f \approx 1.75$. This is in good agreement with the size range in which we observe shear induced hybrid structures in this work. A more detailed comparison of the measured and calculated (ideal) cross over $R_{g,G}$ is given in Table 6. Here, the measured D_f was used in Eq. (6), which had some run to run variation instead of the generic $D_f \approx$ 1.8. Very good agreement is found for the shear initiation time of 15 min. However, for the shear initiation time of 5 min., the agreement is not as good with the calculated value. We should, however, note that $R_{g,G}$ is greatly dependent on any small variation of the fractal dimension as shown in Eq. (6). We also speculate that this difference between theoretical and experimental $R_{g,G}$ for shear initiation time of 5 min. may be due to the fact that the system is not as deep into the cluster dense regime, i.e., it is farther from the gel point, than at 15 min.

$\overline{G}$ (s⁻¹)	Shear initiation time: 5 min.		Shear initiation time: 15 min.	
	Measured $R_{g,G}$ (µm)	Calculated $R_{g,G}$ (µm)	Measured $R_{g,G}$ (µm)	Calculated $R_{g,G}$ (µm)
0.13	-	-	-	-
0.24	-	-	-	-
0.48	-	-	2.8±0.2	2.5±0.5
0.99	-	-	2.0±0.2	2.5±0.5
1.60	1.3±0.1	0.6±0.1	1.9±0.2	1.6±0.3
2.61	1.4±0.2	0.6±0.1	1.3±0.1	1.3±0.2
3.56	1.3±0.1	2.0±0.3	2.2±0.1	2.3±0.4

Table 6: Comparison between the calculated $R_{g,G}$ (µm) and the measured $R_{g,G}$ (µm) at the shear initiation times of 5 and 15 min.

CHAPTER 4 - CONCLUSION

Small angle light scattering was used to study the effect of shear on colloidal aggregates. We showed that shear rates ranging between 0.13 -3.56 s^{-1} could cause different effects, which depended on the shear initiation time and the applied shear rate. When the shear initiation time was 1 min., the aggregation followed the DLCA kinetics regardless of the applied shear rate. At the shear initiation time of 5 min., there were three different behaviors. At low shear rates the gel structure was uniform ($D_f \approx 1.8$), and the gel time was slightly shorter than that from the unsheared gel. At intermediate shear rates there was a hybrid aggregate structure due to the shear; however, Brownian aggregation "repaired" this double structure into a uniform gel structure with a fractal dimension of $D_f \approx 1.8$. At high shear rates the sample reached its gel point due to the shear and the gel time was significantly shorter than the gel time of the no shear situation. When the shear initiation time was 15 min., at all shear rates the sample basically gelled due to the shear. At low shear rates the sample had a uniform gel structure, but at higher shear rates there was a hybrid gel structure.

We now summarize our overall picture of aggregation in our system. The system starts cluster dilute, meaning the average cluster separation to size ratio is much greater than one, and with a Péclet number less than one. Brownian, DLCA aggregation proceeds to make $D_f \approx 1.8$ aggregates. Application of a shear when the aggregates are big enough to yield a Péclet number greater than one results in shear aggregation yielding again $D_f \approx 1.8$. Eventually the system becomes cluster dense through either Brownian or shear aggregation. Shear applied when cluster dense yields larger superaggregates with a hybrid structure of $D_f \approx 2.6$ and 1.8.

REFERENCES

1. J. Goodwin, *Colloids and Interfaces with Surfactants and Polymers* (Wiley, West Sussex, 2004).

2. T. Serra, J. Colomer, and X. Casamitjana, J. Colloid and Interface Sci. **187**, 466 (1997).

3. F. E. Torres, W. B. Russel, and W. R. Schowalter, J. Colloid and Interface Sci. **142**, 554 (1991).

4. T. Serra and X. Casamitjana, J. Colloid and Interface Sci. **206**, 505 (1998).

5. Y. Kikuchi, H. Yamada, H. Kunimori, T. Tsukada, M. Hozawa, C. Yokoyama, and M. Kubo, Langmuir **21**, 3273 (2005).

6. C. Selomulya, G. Bushell, R. Amal, and T. D. Waite, Langmuir **18**, 1974 (2002).

7. M. Y. Lin, R. Klein, H. M Lindsay, D. A. Weitz, R. C. Ball, and P. Meakin, J. Colloid and Interface Sci. **137**, 263 (1990).

8. H. M Lindsay, M. Y. Lin, D. A. Weitz, P. Sheng, Z. Chen, R. Klein, and P. Meakin, Faraday Discuss. Chem. Soc. **83**, 153 (1987).

9. J. E. Martin, J. P. Wilcoxon, D. Schaefer, and J. Odinek, Phys. Rev. A **41**, 4379 (1990).

10. S. J. Jung, R. Amal, and J. A. Raper, Powder Technology **88**, 51 (1996).

11. L. Wang, D. L. Marchisio, R. D. Vigil, and R. O. Fox, J. Colloid and Interface Sci. **282**, 380 (2005).

12. V. Oles, J. Colloid and Interface Sci. **154**, 351 (1991).

13. R. Folkersma, A.J.G. van Diemen, J. Laven, and H.N. Stein, Rheol Acta **38**, 257 (1999).

14. R. C. Sonntag and W. Russel, J. Colloid and Interface Sci. **113**, 399 (1986).

15. J. C. Flesch, P. T. Spicer, and S. E. Pratsinis, Materials, Interfaces and Electrochemical Phenomena **45**, 1114 (1999).

16. P. Varadan and M. J. Solomon, Langmuir **17**, 2918 (2001).

17. C. M. Sorensen, W. Kim, D. Fry, D. Shi, and A. Chakrabarti, Langmuir **19**, 7560 (2003).

18. D. Fry, A. Chakrabarti, W. Kim, and C. M. Sorensen, Phys. Rev. E **69**, 061401 (2004).

19. W. Kim, C. M. Sorensen, D. Fry, and A. Chakrabarti, J. Aerosol Sci. **37***, 386 (2006).

20. L. Cipelletti, S. Manley, R.C. Ball and D. A. Weitz, Phys. Rev. Lett. **84**, 2275 (2000).

21. M. Carpineti and M. Giglio, Phys. Rev. Lett. **68**, 3327 (1992)**; 70**, 3828 (1993).

22. F. Ferri, Rev. Sci. Instrum. **68**, 2265 (1997).

23. C. M. Sorensen, Aerosol Sci. Tech. **35**, 648 (2001).

24. L. Bibette, T.G. Mason, H. Gang, and D.A. Weitz, Phys. Rev. Lett. **69**, 981 (1992).

25. D.J. Robinson and J. C. Earnshaw, Phys. Rev. Lett. **71**, 715 (1993).

26. J. C. Earnshaw, M.B. J. Harrison, and D.J. Robinson, Phys. Rev. E **53**, 6155 (1996).

27. C. Oh and C. M. Sorensen, J. Nanoparticle Research **1**, 369 (1999).

28. H. Huang, C. Oh, and C. M. Sorensen, Phys. Rev. E **57**, 875 (1998).

29. J. J. Cerda, T. Sintes, C. M. Sorensen, and A. Chakrabarti, Phys. Rev. E **70**, 051405 (2004).

30. D. Stauffer, and A. Aharony, *Introduction to Percolation Theory* (Taylor and Francis, London, 1992).

31. J. C. Gimel, T. Nicolai, and D. Durand, J. Sol-Gel Sci. Technol. **15**, 129 (1999).

32. Hasmy and R. Jullien, Phys. Rev. E **53**, 1789 (1996).

33. M. Rottereau, J. C. Gimel, T. Nicolai, and D. Durand, Eur. Phys. J. E **15**, 133 (2004).